

Measurement and analysis of leaded glass polycapillary optic performance for hard x rays

Suparmi, Cari, Lei Wang,^{a)} Hui Wang, W. M. Gibson, and C. A. MacDonald^{b)}

Center for X-Ray Optics, University at Albany, State University of New York, Albany, New York 12222

(Received 1 March 2001; accepted for publication 10 August 2001)

The properties of borosilicate glass polycapillary x-ray optics have been extensively studied. Small-area scatter rejection borosilicate glass polycapillary optics have been demonstrated with good results. Many medical imaging and industrial radiographic applications for x rays would require large-area optics with good scatter rejection. Since shorter optics are easier to manufacture, optics with a shorter length would provide a faster route to bringing the benefit of polycapillary x-ray optics to these applications. Leaded glass would allow the optic to be much shorter and still give good contrast enhancement, because of the superior absorption of lead glass. In order to investigate the feasibility of using leaded glass polycapillary x-ray optics for these applications, measurements and simulations have been performed on the behavior of leaded glass polycapillary fibers in the 9–80 keV energy range. The transmission efficiencies of these fibers of different types and lengths were measured as a function of source location and x-ray energy. The measurements were analyzed using a geometrical optics simulation program, which included roughness, waviness, bending effects, and a leaded glass filter layer. Despite low transmission at low energies, leaded glass polycapillary x-ray optics with a length of 30–60 mm seem promising for many high-energy (>20 keV) x-ray applications. The longer fibers have transmission efficiency of up to 50% in the 35–40 keV, and very low scatter transmission of less than 0.06% up to 80 keV. © 2001 American Institute of Physics. [DOI: 10.1063/1.1408593]

I. INTRODUCTION

Polycapillary optics, consisting of arrays of tiny hollow glass tubes with diameters on the order of a few microns, can be used to control x-ray beams. A polycapillary fiber is a capillary bundle with hundreds or thousands of hollow channels, as shown in Fig. 1. X rays striking the interior of the glass tubes at grazing incidence are guided down the tubes by total external reflection. Arrays of curved or tapered capillaries can be used to focus, collimate, and filter x-ray radiation. Polycapillary optics have potential usefulness in many applications, including x-ray lithography, medical imaging, crystallography, and astronomy.^{1–9}

While properties of borosilicate polycapillary fibers, fabricated optics, and their applications have been studied extensively in the 8–80 keV energy range,^{10–15} leaded glass fiber optics are advantageous for excellent scatter rejection compared to borosilicate glass fibers because of their superior absorption.

In this article, measurement results for a variety of leaded glass single fibers in the energy range from 9 to 80 keV are presented. These fibers have an outer diameter about 0.5 mm, a channel diameter of 12 μm , and an open area from 40% to 60%, as described in Table I. The difference in open area is due to the differences in wall thickness of the hollow tubes which were drawn together to make the fiber, and the differences in the amount of material flow during drawing. The chemical composition of the lead glass is 29.3 wt %

PbO, 45.5% SiO₂, 15.4% K₂O, 5% SrO, and 4.8% BaO with an approximate density of 3.3 g/cm³. The fiber cross sections are hexagonal and the interior is a lattice of rounded hexagons formed as the packed circular tubes were drawn together, as shown in Fig. 1. The letters indicate different batches, which were drawn under different thermal conditions.

The results were analyzed using a geometrical optic simulation program. The use of the simulation to analyze the experimental data from 60-mm-long type-B fibers is demonstrated. Finally, the fitting processes were used to determine the best-fit parameters of the simulation for five other leaded glass fibers. The measurements show the potential for applications at energies from 25 to 80 keV for short-length optics. The analyses from the simulation indicate that waviness and bending are harmful to the transmission at higher energies, and partially blocked channels are more harmful for lower energies.

II. BASIC PRINCIPLE

Capillary x-ray optics use multiple total external reflections to guide grazing-incidence x rays in arrays of tiny hollow glass tubes.¹ For the leaded glass capillaries that were used in the experiments described here, the critical angle for reflectivity is¹⁶

$$\theta_c = 35(\text{mrad})/E(\text{keV}). \quad (1)$$

The higher the photon energy, the smaller is the critical angle.

^{a)}Also at: University of California at Davis, Davis, CA.

^{b)}Electronic mail: c.macdonald@albany.edu

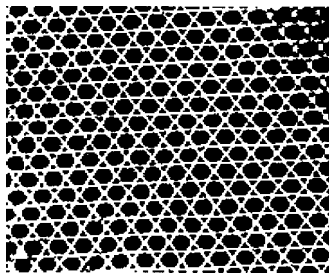


FIG. 1. Photograph of a cross section of a leaded glass polycapillary fiber with channel diameter of $12\ \mu\text{m}$ and fractional open area of 60%.

III. GEOMETRIC SIMULATION

In the geometrical optic simulation used in this article, x-ray transmission through hollow glass fibers is simulated by tracing a large number of x rays through fibers. The simulation includes four fiber quality defects: roughness, waviness, channel blockage, and also profile corrections that can be approximated by uniform bending. It had been shown previously that geometric simulations with these four best parameters are in good agreement with experimental data for borosilicate single fibers at 1–80 keV.^{13,17}

The geometric algorithm is a two-dimensional approximation. Because of the small critical angle, the velocity of the x-ray photon along the capillary axis is nearly equal to c , the velocity of light. The trajectory of an x ray can be reduced to the two-dimensional motion inside the capillary cross section.¹³ Deviations of the channel from a straight path are approximated by uniform bending described by bending radius R . The bending of the channel makes the apparent motion of the x ray within the channel cross section similar to that of a classically accelerated particle.

Surface roughness is formally parametrized by a correlation length and root-mean-square displacement of rough surface z . Because the effect on surface reflectivity of the changes in the correlation length can be compensated by changing the roughness height, and due to the lack of actual correlation data, the correlation length was fixed at $6\ \mu\text{m}$ for all simulations. Changing this value would cause a proportional scaling of all reported roughness heights. The value was chosen for borosilicate fibers so that the roughness heights agree with atomic-force microscopy data.¹³ The surface roughness decreases the apparent reflectivity of the channel walls and, therefore, the transmission in capillary channels.

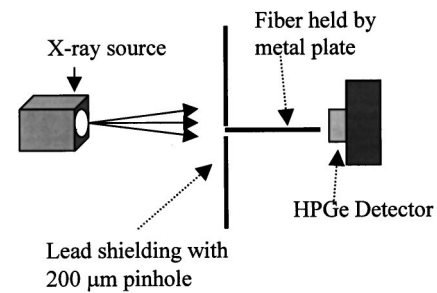


FIG. 2. Scheme of experimental setup for fiber measurement.

The third capillary surface quality parameter is waviness, which occurs on a spatial range shorter than the capillary length and longer than roughness. The average effect of the waviness can be considered as a random tilt of the glass wall. The tilt angles are assumed to be normally distributed with a mean value of zero and a standard deviation w .

The fourth polycapillary defect is channel wall blockage, which is modeled by a filter layer of glass of thickness t . The layer represents glass inclusions which randomly occur along the fiber. The analysis shows that the effects of these four parameters can be easily separated.

IV. EXPERIMENTAL APPARATUS AND TECHNIQUE

A. Experimental apparatus

The experimental apparatus is shown in Fig. 2.

1. Source

The x-ray generator used in the experiment was a low-current Microfocus MS50 with a $50\ \mu\text{m}$ spot size, tungsten target, and a maximum operating voltage of 100 kV. The source head was mounted on a stage which could be moved in the two directions transverse to the x-ray beam. In order to reduce the background of scattered x rays, this movable source was enclosed in a 6-mm-thick lead box with a $100 \times 175\ \text{mm}$ aperture in the front. The source-to-fiber distance was 1100 mm. In the measurement for photons with energy higher than 50 keV, a 5-mm-thick aluminum plate was used as a filter between the source and the fiber to remove the low-energy photons, and reduce the dead time of the detector.

TABLE I. Fiber descriptions and best-fit simulation parameters from Secs. V B and V C.

Fiber type	Fiber description			Best-fit simulation parameters				
	Outer diameter mm	Channel size μm	Open area %	Length mm	Bending R m	Waviness w mrad	Layer t μm	Roughness z nm
A	0.53	12	60	60	40	0.26	45	1.8
B30	0.51	12	60	30	30	0.15	18	1.7
B60	0.51	12	60	60	56	0.15	33	1.7
C	0.51	11	50	60	27	0.19	33	1.8
D	0.53	11	50	60	28	0.20	43	1.8
E	0.53	11	40	60	45	0.28	47	2.1

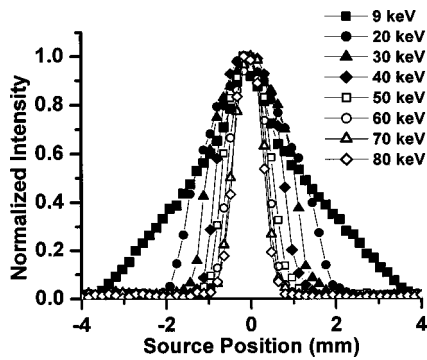


FIG. 3. Normalized transmission vs source position, taken by moving the source in the horizontal direction traverse to fiber axis with the fiber, pinhole, and detector fixed.

2. Pinhole

A 200- μm -diam pinhole through 4 mm of lead, 2 mm tungsten, and 1 mm of tantalum (attached together), was placed 5 mm away from the fiber at the entrance end. The pinhole was attached to a 6-mm-thick lead shield. The pinhole and lead shield together block scattered x rays and leakage around the outside of the fiber. The pinhole was smaller than the fiber but still covers hundreds or more channels. Its small size was chosen not only to avoid the leakage around the fiber and reduce dead time in the detector, but also to keep the source–fiber distance as small as possible while keeping the photon entrance angle at the edges of the pinhole to less than the critical angle at energies up to 80 keV.

3. Fiber

The fiber was held straight by a finely machined groove in an aluminum plate and covered by iron powder to prevent x-ray leakage around the fiber. The aluminum plate was also mounted on a stage which can be translated in two orthogonal directions transverse to the beam. All stages were mounted on rail carriers which could be moved along the beam directions. Five kinds of fibers, listed in Table I, were measured.

4. Detector

The detector was a high-purity germanium detector with about 200 eV resolution at 5.9 keV and 550 eV at 122 keV. The detector was placed behind the fiber. The distance between the source and detector was fixed to keep air absorption constant. Motion control and data collection were all performed with a small computer.

V. MEASUREMENT RESULTS AND ANALYSIS

A. High-angle transmission

Source scan plots of transmission through a type-B60 fiber as a function of source location, for seven different energy windows of approximately 2 keV in width, are shown in Fig. 3. The transmission plots are narrower for the higher-energy windows, as expected due to the decrease in critical angle with photon energy. For leaded glass fibers, because of the high absorption of lead, the background signal from pho-

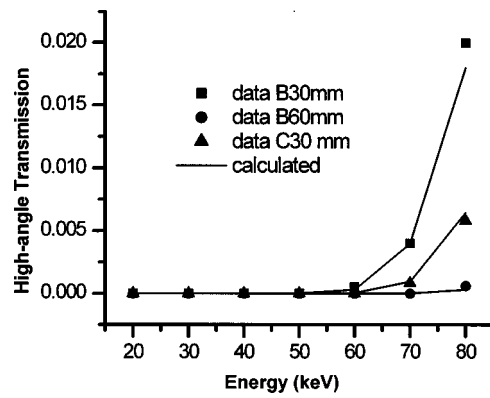


FIG. 4. High-angle (cut through) transmission vs energy, measured with the source moved away from the aligned position to an angle larger than the critical angle. Lines are theoretical calculations using Eq. (2).

tons with incidence angle greater than the critical angle is very small. These photons are absorbed, rather than cutting through the glass wall. The cut through transmission is 3.6% at 80 keV for a 30-mm-long type-B fiber and 0.18% for a 60-mm-long fiber. Measured and theoretical high-angle transmission at several energies are shown in Fig. 4. The theoretical values are calculated using¹³

$$T_c = e^{-\ell(1-f)\mu}, \tag{2}$$

where ℓ is the fiber length, f is the fractional open area of the fiber, ρ is the density of the glass, and μ is the attenuation coefficient of the glass obtained from the tabulated values.¹⁸ The transmission results which follow are channel transmissions from which the very small high-angle cut through and fluorescence background have been subtracted.

B. Simulation analysis

Transmission for the leaded glass fibers in Table I was measured in the energy range of 9–80 keV. To illustrate the effect of each simulation parameter, the application of the simulation to the experimental data for fiber type-B60 (a 60-mm-long type-B fiber) is discussed in this section.

1. Bending effects

A slight bending can dramatically reduce the transmission at the high energies where the critical angles are small-

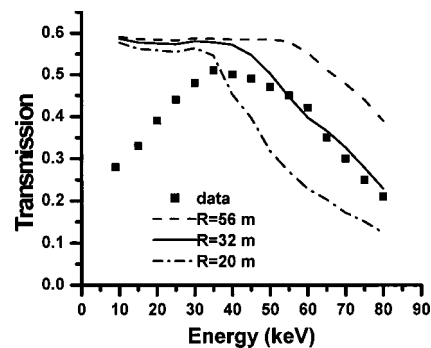


FIG. 5. Simulated transmission spectra (lines) of a type B60 fiber for different bending radii are compared with the experimental data (boxes). The figure shows that bending alone cannot fit the data since the sharpest bend underestimates the transmission at high energies.

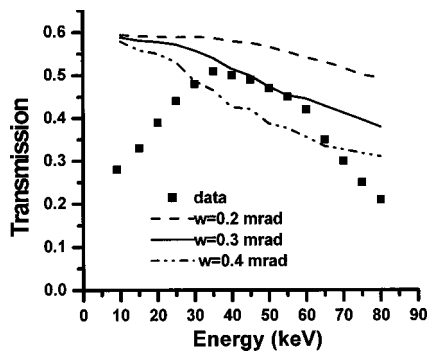


FIG. 6. Simulated transmission spectra (lines) of a type B60 fiber for different wavinesses are compared with the experimental data (boxes). The waviness correction causes the transmission to drop primarily in the middle-energy range.

est. The measured transmission as a function of energy along with the simulations with different bending radii for fiber type B60 is shown in Fig. 5. The simulation with bending along cannot fit the experimental data since at the smallest radius the transmission is too high at low energies and too low at high energies. Since any waviness correction will reduce the transmission, the radius of bending has to be larger than 32 m.

2. Waviness effects

Simulations with different waviness corrections are compared to the experimental data of transmission spectra for a type-B60 fiber in Fig. 6. The waviness alone cannot fit the data. The simulation shows that the waviness causes the transmission to drop rapidly at medium energies but not rapidly enough at higher energies. Figure 6 shows that the waviness correction has to be smaller than 0.3 mrad to fit the data. Simulated transmission source scans with different waviness are compared to the experimental data at 40 keV in Fig. 7. The simulation with a waviness of 0.15 mrad fits the spectrum source scan fairly well at 40 keV. Thus, the maximum value of waviness is 0.15 mrad.

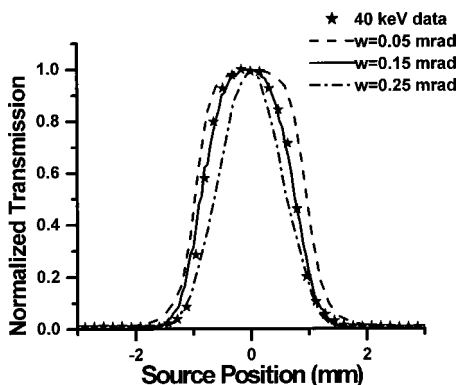


FIG. 7. Simulated source scan curves (lines) with different wavinesses are compared with the experimental data (stars) at 40 keV. Since the simulated curve with a waviness of 0.15 mrad fits the data fairly well, it is used as the value for waviness in the best-fit simulation parameters in Table I.

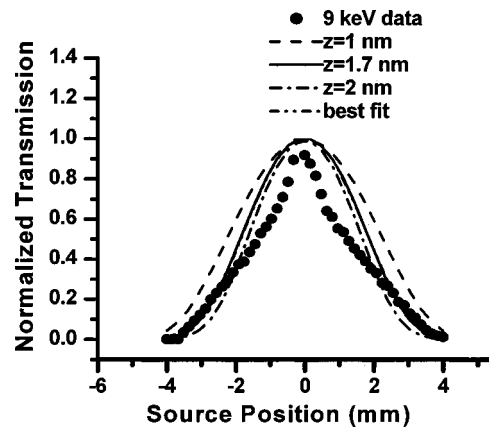


FIG. 8. Simulated source scan curves (lines) for a type B60 fiber for different roughnesses are compared with experimental data (circles) at 9 keV. The curve is too low at large displacements for the highest value of roughness. For all values of roughness the curve is too wide at small displacements even for the best-fit simulation, using in addition to $z=1.7$ nm, the bending and waviness from Table I. This may be because the actual unnormalized transmission at 9 keV is quite low.

3. Roughness effects

Roughness has only a fairly small effect on the transmission spectrum. The transmission drop depends on both the surface reflectivity, which is slightly reduced by roughness, and the number of reflections that the photon undergoes through the channel, since the transmission is approximately proportional to R^n , where R is the reflectivity, and n is the number of bounces. For a straight capillary with the source aligned, the average number of bounces of the photon along the channel is small, usually less than 3, and the roughness has little effect. The transmission is more affected if the source is off axis. The transmission as a function of source displacement is shown in Fig. 8. Because photons experience more than 21 reflections for large source displacements, the transmission at high angles is sensitive to roughness and becomes too small if the roughness is larger than 1.7 nm. The best-fit parameter is taken as $z=1.7$ nm.

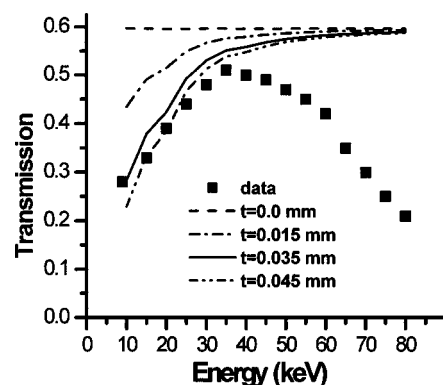


FIG. 9. Simulated transmission spectra (lines) with different layer thicknesses alone compared with the experimental data (boxes). The figure shows that the maximum layer thickness for a type B60 fiber is 35 μm to fit the low-energy transmission.

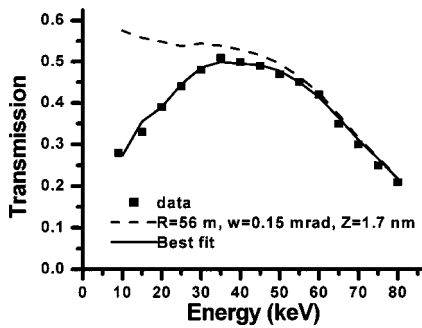


FIG. 10. Simulated transmissions with (solid line) and without (dashed line) a leaded glass filter layer for a type B60 fiber are compared with the experimental data (boxes). Best fit is achieved with $R=56$ m, $w=0.15$ mrad, $z=1.7$ nm, $s=6$ μ m, and $t=33$ μ m.

4. Channel blockage

The drop in transmission at low energies can be fit by modeling channel blockage with a glass filter layer of thickness t . The simulated transmission spectra with different layer thicknesses is compared with the experimental data in Fig. 9.

5. Best fit

To fit the transmission spectrum data, finally, we combine the waviness determined from the source scan curve at 40 keV, the roughness determined from the source scan curve at 9 keV, and add the bending radius and a glass layer which from Fig. 9 must be less than 35 μ m. Figure 10 shows that the inclusion of a 33- μ m-thick glass layer gives a good fit with the experimental transmission spectrum. The simulation with the four best-fit simulation parameters is compared to the experimental source scans in Fig. 11. The simulated transmission spectra and source scans at medium and high energies fit the data fairly well.

The primary effect of bending is to reduce the transmission at highest energies. Channel blockage reduces the transmission at lowest energies. Roughness reduces the width of the source scan width at these low energies. Waviness reduces the transmission and the source scan width at midrange energies.

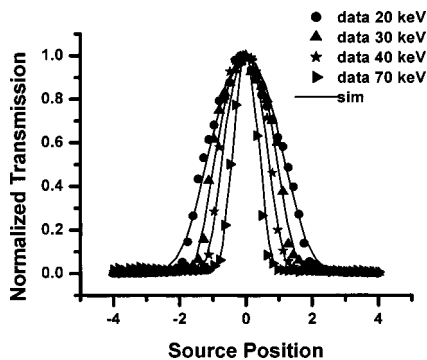


FIG. 11. Simulated scan curves with best-fit simulation parameters for a type B60 fiber compared with the experimental data at four photon energies.

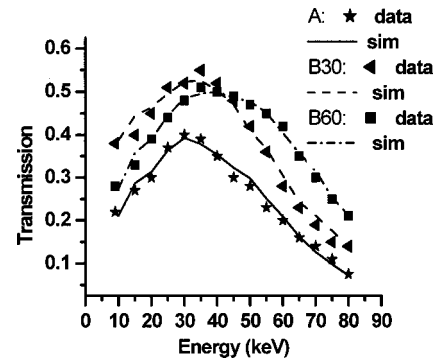


FIG. 12. Simulation of transmission spectra of fiber A, fiber B60 (B with length of 60 mm), and fiber B30 (B with length of 30 mm) with their best-fit parameters listed in Table I, compared with the experimental data.

C. Explanation of the experiment results

Using the fitting processes described in Sec. V B, the best-fit simulation parameters for fibers A, C, B60, D, and E, which have a length of 60 mm, and also fiber B30, which has a length of 30 mm, were obtained. The best-fit simulation parameters are listed in Table I. The best-fit simulated transmissions along with the experimental data are shown in Fig. 12 and 13. The outer diameters of the fibers are in the 0.51–0.53 mm range. These fibers are thin and flexible, and therefore, are difficult to keep straight in the measurement apparatus, resulting in sharp bending radii and relatively poor high-energy transmission. All the fibers have a similar roughness. Fiber type B has a high open area, low channel blockage, and the least bending and waviness. Thus, this fiber has better transmission than other fibers.

Fiber A has more waviness and more glass inclusions, and thus poorer transmission at all energies. Waviness arises from sensitivity to vibration during the fiber pulling processes, and both manufacturing defects are affected by detailed thermal history. Fibers C, D, and E have a lower open area, which reduces the maximum possible transmission. Fiber types C and D have the same open area, but fiber type C has a thinner glass layer. As a result, fiber type C has a higher transmission at lower energies than fiber type D, as shown in Fig. 13.

Figure 12 shows that the transmission of fiber type B with the shorter length is higher at lower energies than the longer length fiber because of its thinner blockage layer. The

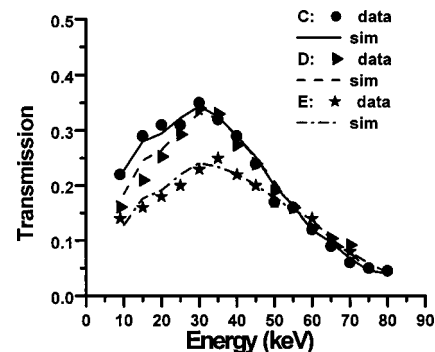


FIG. 13. Simulated transmission spectra of fibers C, D, and E with their best-fit parameters listed in Table I, compared with the experimental data.

thinner layer is consistent with a statistically random model of glass inclusion. However, because of its high flexibility, the shorter fiber experiences more bending than the longer fiber, and thus the transmission falls off faster at higher energies. Because the bending radius of the fiber is proportional to the square of the fiber length, even if the shorter fiber experiences a smaller deflection than the longer fiber, the shorter fiber still can have a smaller bending radius.¹³ The bending is due to residual stress in the glass. Because the longer fiber is heavier it resists being lifted out of the groove by the residual stress.

VI. CONCLUSIONS

The measured transmission is greater than 45% for fiber type B in the 25–50 keV energy range. The geometric simulation, with roughness, waviness, bending, and channel blockage corrections, performs well in explaining the measured transmission spectra. According to this simulation, bending is the most harmful at higher energies, and glass inclusions that block the channels are harmful at lower energies. The high-energy transmission performance could be improved by making the fibers larger in diameter, and therefore more rigid, to minimize unintentional bending. Low-energy performance would be improved by using shorter fibers. Because of the good absorption of lead, the high-energy photons which are not reflected are absorbed nearly completely by 60-mm-long fibers, even at 80 keV. The high-angle transmission at 80 keV is only 0.2%. At energies below 50 keV, the high-angle transmission is negligible for the 30 mm length. Thus, short leaded glass polycapillary x-ray optics are very promising for scatter rejection applications.

ACKNOWLEDGMENTS

The authors wish to acknowledge assistance from Michael Gubarev, Frank Hoffman, Christine Russel, C. A.

Freinberg-Trufas, Francisca Sugiro, and Sushil Padiyar. This work was supported by Department of Army Breast Cancer Research Project Grant No. DAMD 17-97-1-7304, and NIH Grant Nos. RO1 CA77477-01, CA58521-05, and I 43 CA58146-01.

- ¹W. M. Gibson, C. A. MacDonald, and M. A. Kumakhov, *Proc. IEEE* **2580**, 164 (1991).
- ²C. A. MacDonald, *J. X-Ray Sci. Technol.* **6**, 32 (1996).
- ³D. G. Kruger, C. C. Abreu, E. G. Hendee, A. Kocharian, W. W. Pepler, C. A. Mistretta, and C. A. MacDonald, *Med. Phys.* **23**, 187 (1996).
- ⁴C. C. Abreu and C. A. MacDonald, *Phys. Medica* **XIII**, 79 (1997).
- ⁵C. A. MacDonald, S. M. Owens, and W. M. Gibson, *J. Appl. Crystallogr.* **32**, 160 (1999).
- ⁶S. M. Jorgensen, D. A. Rayes, C. A. MacDonald, and E. L. Ritman, *Proc. SPIE* **3772**, 158 (1999).
- ⁷F. A. Hofmann, W. M. Gibson, C. A. MacDonald, D. A. Carter, J. X. Ho, and J. R. Ruble, *J. Appl. Cryst.* **34**, 330 (2001).
- ⁸C. H. Russel, M. Gubarev, J. Kolodziejczak, M. Joy, C. A. MacDonald, and W. M. Gibson, *Adv. X-Ray Anal.* **43** (1999).
- ⁹L. Wang, C. A. MacDonald, and W. W. Pepler, *Med. Phys.* (to be published).
- ¹⁰C. A. MacDonald, C. C. Abreu, S. Budkov, H. Chen, X. Fu, W. M. Gibson, Kardiawarman, A. Karnaukhov, V. Kovantsev, I. Ponomarev, B. K. Rath, J. B. Ullrich, M. Vartanian, and Q. F. Xiao, *Proc. SPIE* **2011**, 275 (1993).
- ¹¹J. B. Ullrich, V. Kovantsev, and C. A. MacDonald, *J. Appl. Phys.* **74**, 5933 (1993).
- ¹²C. C. Abreu, D. G. Kruger, C. A. MacDonald, C. A. Mistretta, W. W. Pepler, and Q. Xiao, *Med. Phys.* **22**, 1793 (1995).
- ¹³L. Wang, B. K. Rath, W. M. Gibson, J. C. Kimball, and C. A. MacDonald, *J. Appl. Phys.* **80**, 3628 (1996).
- ¹⁴F. A. Hofmann, C. A. Freinberg-Truffas, S. M. Osens, S. D. Padiyar, and C. A. MacDonald, *Nucl. Instrum. Methods Phys. Res. B* **133**, 145 (1997).
- ¹⁵B. K. Rath, W. M. Gibson, L. Wang, B. E. Homan, and C. A. MacDonald, *J. Appl. Phys.* **83**, 7424 (1998).
- ¹⁶J. D. Jackson, *Classical Electrodynamics* (Wiley, New York, 1962), Sec. 7.9, p. 227.
- ¹⁷H. Wang, L. Wang, W. M. Gibson, and C. A. MacDonald, *Proc. SPIE* **3444**, 643 (1998).
- ¹⁸The NNDC online data service, Brookhaven National Laboratory Nuclear Data Center (Remote host address: bnln2.dne.bnl.gov).